Title: Single voxel autocorrelation uncovers gradients of temporal dynamics in the hippocampus and entorhinal cortex during rest and navigation

Authors: Nichole R. Bouffard*[1,2], Ali Golestani*[1], Iva K. Brunec[3], Buddhika Bellana[1,4], Morgan D. Barense†[1,2], Morris Moscovitch†[1,2]

* These authors contributed equally

† Shared senior authorship

Affiliations

[1]Department of Psychology, University of Toronto, Toronto, Ontario, Canada

[2]Rotman Research Institute, Baycrest Health Sciences, North York, Ontario, Canada

[3]Department of Psychology, Temple University, Philadelphia, Pennsylvania, USA

[4]Department of Psychology, Glendon College - York University, Toronto, Ontario, Canada

Abstract

During navigation, information at multiple scales needs to be integrated. Single-unit recordings in rodents suggest that gradients of temporal dynamics in the hippocampus and entorhinal cortex support this integration. In humans, gradients of representation are observed, such that granularity of information represented increases along the long axis of the hippocampus. The neural underpinnings of this gradient in humans, however, are still unknown. Current research is limited by coarse fMRI analysis techniques that obscure the activity of individual voxels, preventing investigation of how moment-to-moment changes in brain signal are organized and how they are related to behavior. Here, we measured the signal stability of single voxels over time to uncover previously unappreciated gradients of temporal dynamics in the hippocampus and entorhinal cortex. Using our novel, single voxel autocorrelation technique, we show for the first time a medial-lateral hippocampal gradient, as well as a continuous autocorrelation gradient along the anterolateral-posteromedial entorhinal extent. Importantly, we show that anterior-posterior and medial-lateral hippocampal autocorrelation gradients were modulated by navigational difficulty, indicating that changes in signal stability are relevant for behavior. Our method and findings open the door for future research on how temporal gradients within these structures support the integration of information for goal-directed behavior.

Acknowledgments

We thank Menno Witter for his feedback on an earlier draft of this paper. Dataset 1 was provided by the Human Connectome Project, WU-Minn Consortium (Principal Investigators: David Van Essen and Kamil Ugurbil; 1U54MH091657) funded by the 16 NIH Institutes and Centers that support the NIH Blueprint for Neuroscience Research; and by the McDonnell Center for Systems Neuroscience at Washington University. We thank Jason Ozubko for his contributions to the experiment conceptualization of and data collection for Dataset 2. MDB was supported by the Natural Sciences and Engineering Research Council Discovery Grant (RGPIN-2020-05747), a James S McDonnell Scholar Award, an Early Researcher Award from the Ontario Ministry of Development and Innovation, and a Canada Research Chair. MM was supported by the Canadian Institutes of Health Research Grant (MOP 125958).

Conflict of interest statement

The authors declare no competing financial interests.

Introduction

To enable efficient goal-directed behaviour, information must be represented and integrated across multiple temporal and spatial scales. It has been proposed that neural signal gradients in the hippocampus and entorhinal cortex support such multi-scale representations in rodents, but evidence in humans is sparse and has methodological limitations. Previously, fMRI analysis techniques have uncovered local signal gradients in the human hippocampus (Brunec, Bellana, et al., 2018). These investigations, however, have been limited by analyzing patterns of activity across relatively coarse regions of interest, making it unclear how sustained versus rapidly changing signals are distributed throughout the hippocampus. Many of these analyses use predetermined anterior and posterior anatomical masks, which limit our ability to detect neural signal gradients in an unsupervised way, therefore preventing us from investigating gradients that exist along both anterior-posterior and medial-lateral axes of the hippocampus. Moreover, there have been no prior investigations of autocorrelation gradients in the entorhinal cortex, despite evidence of its role in spatial and temporal representations during navigation. To address these limitations, we have developed a novel, data-driven analysis based on autocorrelation of single voxels in fMRI during rest and navigation. This technique allows us, for the first time, to track the signal stability of individual voxels and their spatial distribution in an unconstrained way along both the anterior-posterior and medial-lateral axes of the hippocampus and entorhinal cortex. Based on this single voxel analysis we uncover gradients of neural signal dynamics along these axes in both structures and relate them to behavior.

In rodents, place fields in the ventral hippocampus (homologous to the anterior hippocampus in humans) span larger areas, show a higher degree of overlap, and higher correlation in their firing across time, compared to the dorsal hippocampus (homologous to the posterior hippocampus in humans) (Hasselmo, 2008; Jung et al., 1994; Kjelstrup et al., 2008; Komorowski et al., 2013). A similar gradient of hippocampal organization is also observed in the human hippocampus. Tracking moment-to-moment similarity across patterns of voxels during virtual navigation, Brunec, Bellana, et al. (2018) found that signal similarity was significantly greater within the anterior hippocampus relative to the posterior hippocampus, indicating that, as in the rodent ventral hippocampus, the human anterior hippocampus demonstrates slower changing signals that are sustained across time and space. These results suggest that a relatively stable pattern of activity in the rodent and human hippocampus follows a scaled gradient, from faster changing signal in the posterior (dorsal) hippocampus to slower changing

signal in the anterior (ventral) hippocampus. This gradient organization might underlie fine-to-coarse mnemonic representation, particularly when a different granularity of information needs to be maintained across time (Brunec & Momennejad, 2019; Robin & Moscovitch, 2017). In addition to the dorsal-ventral gradient of spatial representation observed in rodents, research suggests a difference in spatial selectivity along the proximodistal axis (homologous to medial-lateral in humans), specifically in CA1 (Igarashi et al., 2014), yet whether a similar medial-lateral distinction exists in the human hippocampus is still unclear (Hrybouski et al., 2019).

A key input structure to the hippocampus that has been implicated in integrating information over time during navigation is the entorhinal cortex. Prior research has found distinct functional differentiation between the anterolateral and posterior-medial aspects of the entorhinal cortex (ERC), but there have been no prior investigations of neural signal gradients in the ERC. The lateral ERC in rodents, and the homologous anterolateral ERC in humans, supports within-object and object-location coding, as well as temporal information processing (Bellmund et al., 2019; Montchal et al., 2019; Olsen et al., 2017; Tsao et al., 2018; Yeung et al., 2017; 2019). In contrast, the posteromedial ERC in humans, has been primarily linked to scene processing (Berron et al., 2018; Maass et al., 2015; Navarro Schröder et al., 2015) and related to grid cell organization (Bellmund et al., 2016), consistent with evidence of grid cells in the medial ERC in rodents (Hafting et al., 2005). Given prior evidence of functional distinctions of the ERC into anterolateral and posteromedial regions, we developed a data-driven method to investigate directly, a continuous neural signal gradient in both the anterior-posterior and medial-lateral axes of this structure.

To understand how a graded organization of signal dynamics in the hippocampus and ERC supports goal-directed behavior, we developed an analytic approach of temporal autocorrelation at the single voxel level, which we implemented during both rest and navigation. Temporal autocorrelation represents the degree of similarity between a signal and the temporally shifted, or lagged, version of the signal over successive time intervals (Figure 1A). Conventionally, it is assumed that this autocorrelation in fMRI data originates from physical and physiological noise (Arbabshirani et al., 2014; Bollmann et al., 2018; Bullmore et al., 2001; James et al., 2019; Lenoski et al., 2008; Lund et al., 2006; Purdon & Weisskoff, 1998) or the hemodynamic response function (Arbabshirani et al., 2014; James et al., 2019; Rajapakse et al., 1998) and, therefore, has been considered irrelevant to brain function. Recently, however, Arbabshirani et al. (2019) found that autocorrelation reflects changes in cognitive state (task vs. rest) as well as

changes in mental state (healthy control vs. schizophrenia), suggesting that the observed changes in the autocorrelation are also modulated by cognitive processes. Prior studies, however, have been limited and are unable to answer the question of how temporal autocorrelation is directly related to behavior. Examining the temporal autocorrelation of single voxels during an active navigation task, therefore, is important for understanding how a stable, highly correlated signal is relevant for behavior.

Investigating the fMRI signal at the single voxel level allows us to measure neural gradients with more precision than previous methods. While studies with fMRI in humans suggest that functional heterogeneity exists along the long axis of the hippocampus (Nadel et al., 2013; Poppenk et al., 2013; see Grady, 2020 for a review) and medial-lateral extent of the ERC (e.g., Hafting et al., 2005; Maass et al., 2015; Navarro Schröder et al., 2015), previous analysis techniques have been limited to investigations using predetermined anatomical masks, which obscures the contribution of individual voxels, making it unclear whether graded signals extend along multiple axes in these regions. Furthermore, examining the autocorrelation at the single voxel level allows for a finer-grained analysis that may be more sensitive to differences in navigational performance and can help us to determine how a scaled gradient of signal similarity might be employed to integrate representations across spatial scales during navigation. We, therefore, combine our single voxel autocorrelation approach with an unconstrained clustering method to determine how temporal autocorrelation is distributed in multiple dimensions throughout the hippocampus and ERC.

Here we present the first evidence of a medial-lateral neural signal gradient in the hippocampus as well as a novel continuous gradient in the ERC. Using resting state fMRI data with high spatial and temporal resolution from the Human Connectome Project (HCP), we measured single voxel autocorrelation in the hippocampus and ERC. Specifically, we measured the similarity of single voxels over time by correlating the timecourse of each voxel with temporally shifted versions of itself (Figure 1A). We applied data-driven clustering to determine how temporal autocorrelation was spatially distributed throughout the hippocampus and ERC. We found high autocorrelation in the anterior-medial hippocampus and posteromedial ERC and low autocorrelation in the posterior-lateral hippocampus and anterolateral ERC. Using task-based fMRI, we replicated these results and also demonstrated that increases in navigation difficulty were associated with increases in autocorrelation in the anterior-medial hippocampus. Our single voxel autocorrelation approach yields consistent and precise gradients of single voxel autocorrelation in the hippocampus and ERC, providing a powerful new

continuous and data-driven method that can illuminate how temporal dynamics in brain signals relate to complex cognition.

Results

Dataset 1: Resting state fMRI

Hippocampus

Spatial distribution of single voxel autocorrelation

To examine hippocampal dynamics at the single voxel level when no cognitive demands were placed on participants, we first analyzed resting-state fMRI data from 44 participants from the Human Connectome Project (HCP) Retest dataset (2 runs per participant). Here, we correlated the timecourse of activity of each voxel in the hippocampus with activity in that same voxel shifted by a temporal lag of 1 TR (Dataset 1 TR = 720 ms). We repeated this process until a maximum temporal shift of 4 seconds was reached, or 5 lags (Figure 1A). A map of single voxel autocorrelation values throughout the hippocampus was generated for each lag separately (for a theoretical schematic, see Figure 1B).

We found that single voxel autocorrelation maps at the group level (lags 1-5) showed a notable difference in the distribution of single voxel autocorrelation values along the hippocampal axis (Figure 2A). More specifically, voxels with higher single voxel autocorrelation were mainly in the anterior-medial region whereas voxels with lower single voxel autocorrelation were mainly in the posterior-lateral region (in both left and right hippocampus). As shown in Figure 2A, although the overall autocorrelation decreased as the lag increased, the overall pattern of autocorrelation gradients was similar for lags 1-5.

Single voxel autocorrelation – Reliability results

We next tested the reliability of these results. Here we defined a reliable result as one in which single voxel autocorrelation vectors generated from two runs of the *same* participant were more similar than two runs from *different* participants (lower intra-subject Euclidean distances compared to inter-subject Euclidean distances). Nonparametric permutation tests comparing intra-subject and inter-subject Euclidean distance revealed reliable results in both the left (intra-subject: 7.43 ± 2.07, inter-subject: 9.38 ± 2.22, $P < 0.0001$) and right hippocampus (intra-subject: 7.22 ± 1.98, inter-subject: 9.02 ± 2.02, $P < 0.0001$) (Figure 3A). These high intra-subject similarity values suggest that the single voxel autocorrelation pattern is an intrinsic feature of the brain, likely originating from neuronal sources, rather than noise or imaging artifacts.

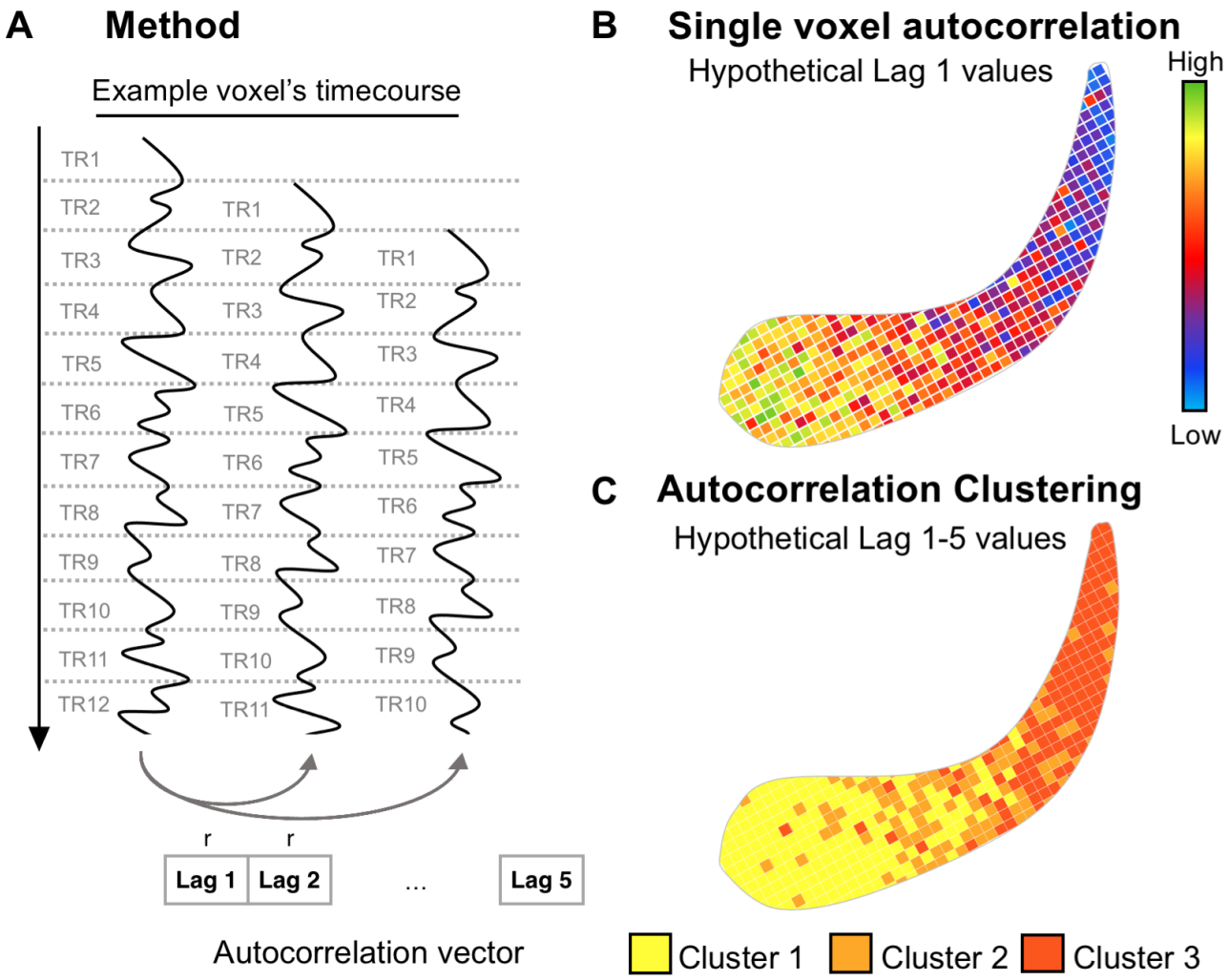

Figure 1. A) Method. For each voxel, the timecourse of activity was successively temporally shifted by 1 TR and correlated with itself. This was repeated for a total shift of 4 seconds (i.e., 5 lags for resting state data (Dataset 1) and 2 lags for navigation data (Dataset 2)). This resulted in a vector of single voxel autocorrelation values, with each value corresponding to a different lagged correlation. **B) Single voxel autocorrelation (hypothetical values).** The procedure was repeated for all voxels in an ROI. To examine the spatial distribution of the single voxel autocorrelation, we plot the group-level single voxel autocorrelation maps for each lag, averaged across runs and participants. **C) Autocorrelation clustering (hypothetical values).** The autocorrelation values for each lag were stored in a vector (single voxel autocorrelation vector). The voxels in the ROI were clustered based on the similarity (Euclidean distance) of single voxel autocorrelation vectors. Single voxel autocorrelation vectors were clustered according to their Euclidean distance (Blondel et al., 2008). Clustering was performed at the individual-level and at the group-level.

Autocorrelation Clustering

We applied a Louvain clustering method using modularity maximization without predefining the number of clusters (Blondel et al., 2008) to the group-level single voxel autocorrelation vectors (for a theoretical schematic, see Figure 1C). This data-driven clustering approach revealed three distinct clusters in both the left and right hippocampus (Figure 2B); notably, past work that segmented the hippocampus into two ROIs (anterior and posterior) a priori would not have been able to detect the presence of this third cluster. Consistently across all 5 lags we found that Cluster 1 had the highest single voxel autocorrelation values and was located in the anterior-medial hippocampus (Figure 2D). Cluster 3 had the lowest single voxel autocorrelation values and was located in the posterior-lateral part of the hippocampus. Cluster 2 had intermediate single voxel autocorrelation values and was located between Clusters 1 and 3. These three clusters were also reliably observed at the individual level (cluster maps from two runs of an example participant are shown in Figure 2B).

In summary, clustering revealed a high-to-low single voxel autocorrelation gradient along the anterior-posterior axis, consistent with what has been previously found in the literature (Brunec, Bellana, et al., 2018; Raut et al., 2020). In addition, we found differences along the medial-lateral axis, as well as a prominent anterior-medial cluster of high single voxel autocorrelation that could be distinguished from a posterior-lateral cluster of low single voxel autocorrelation. While previous methods using predetermined anterior/posterior ROI masks might have missed this medial-lateral distinction, our data-driven method provides evidence that an autocorrelation gradient exists along multiple spatial dimensions.

Autocorrelation Clustering – Reliability results

The reliability of single voxel autocorrelation clustering was evaluated by measuring spatial overlap between clusters, calculated by the Jaccard coefficient (Figure 3B). Here we defined a reliable result as one in which the spatial distribution of autocorrelation clusters was consistent across the two runs of the same participant, indicated by greater overlap (higher Jaccard coefficient) among clusters *within* an individual compared to *between* different individuals. Using nonparametric permutation, we found high reliability for clusters in the bilateral hippocampus, specifically Cluster 1 (Left: $P < 0.001$; Right: $P < 0.001$) and Cluster 3 (Left: $P < 0.001$; Right: $P < 0.001$). These findings of high intra- and inter-subject overlap suggest that Clusters 1 and 3 were highly reliable, within individuals. Cluster 2, however, had significantly lower overlap (Left: $P = 0.06$; Right: $P = 0.007$), suggesting more variability within individuals.

Gradients of single voxel autocorrelation (lag 1)

The single voxel autocorrelation and autocorrelation clustering results presented above both suggest the presence of an autocorrelation gradient along two main axes: the anterior-posterior axis and the medial-lateral axis. To more precisely examine these individual gradients, we plotted the single voxel autocorrelation across hippocampal slices along the X (medial-lateral), Y (posterior-anterior), and Z (inferior-superior) axes. We observed consistent gradients in every participant. Specifically, single voxel autocorrelation gradually decreased in the medial-to lateral direction and increased in the posterior-to-anterior direction (Figure 2C; we focused on lag 1, but a similar pattern was revealed across all lags, as shown in Figure 2A). A rough gradient of high-to-low autocorrelation was also observed in the inferior-superior axis, which is due to the angle of the hippocampus (i.e., the anterior hippocampus is located more inferiorly relative to the posterior hippocampus). When we investigated the spatial distribution of the three clusters (projected on the background of the plots in Figure 2C), we observed a gradient of cluster assignment that complemented the single voxel autocorrelation gradients. Specifically, high-to-low single voxel autocorrelation gradients were also associated with a cluster gradient from Cluster 1 to Cluster 3.

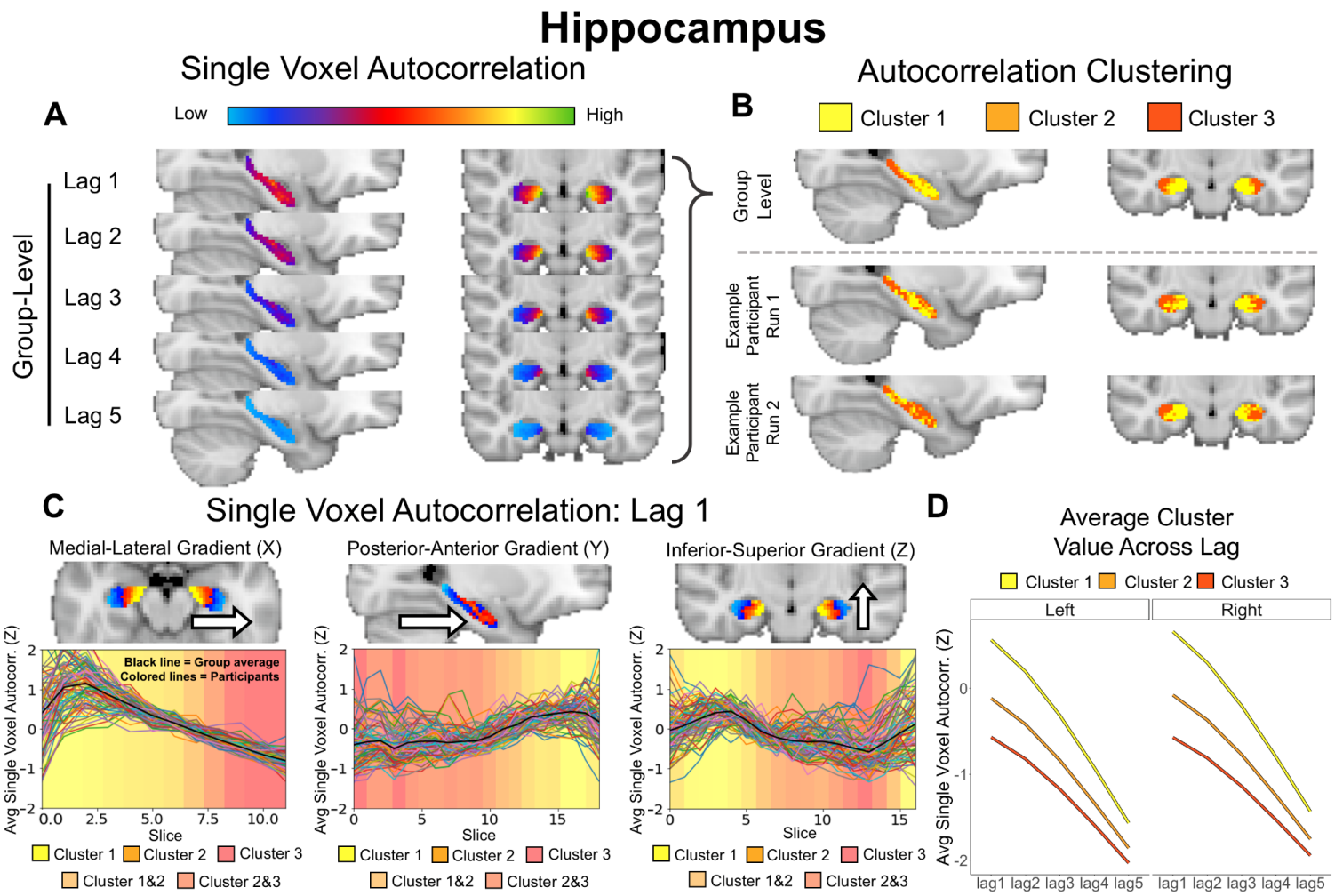

Figure 2. Hippocampus. Single Voxel Autocorrelation. A) Group-level single voxel autocorrelation maps averaged across all runs for all participants. **Autocorrelation Clustering. B)** Group-level clusters (top) and run-level cluster maps for two runs from an example participant (bottom). Three distinct clusters were found at both the group and the individual run-level. Cluster 1 was located in the anterior-medial hippocampus, Cluster 3 was located in the posterior-lateral hippocampus, and Cluster 2 was located between Cluster 1 and 3. **C) Single Voxel Autocorrelation: Lag 1.** Single voxel autocorrelation (lag 1) averaged per slice and projected into three axes (X, Y, and Z) to visualize changes in medial-lateral, anterior-posterior, and inferior-superior directions (plots depict left hemisphere; right hemisphere looked similar). The average cluster assignment of voxels on each slice is presented as the background color to show the gradation in values along the three axes. **D) Average Cluster Value Across Lag.** Average group-level single voxel autocorrelation values for each cluster at each lag. Cluster 1 was associated with the highest single voxel autocorrelation values, Cluster 2 with intermediate values, and Cluster 3 with the lowest. This was consistent across all 5 lags.

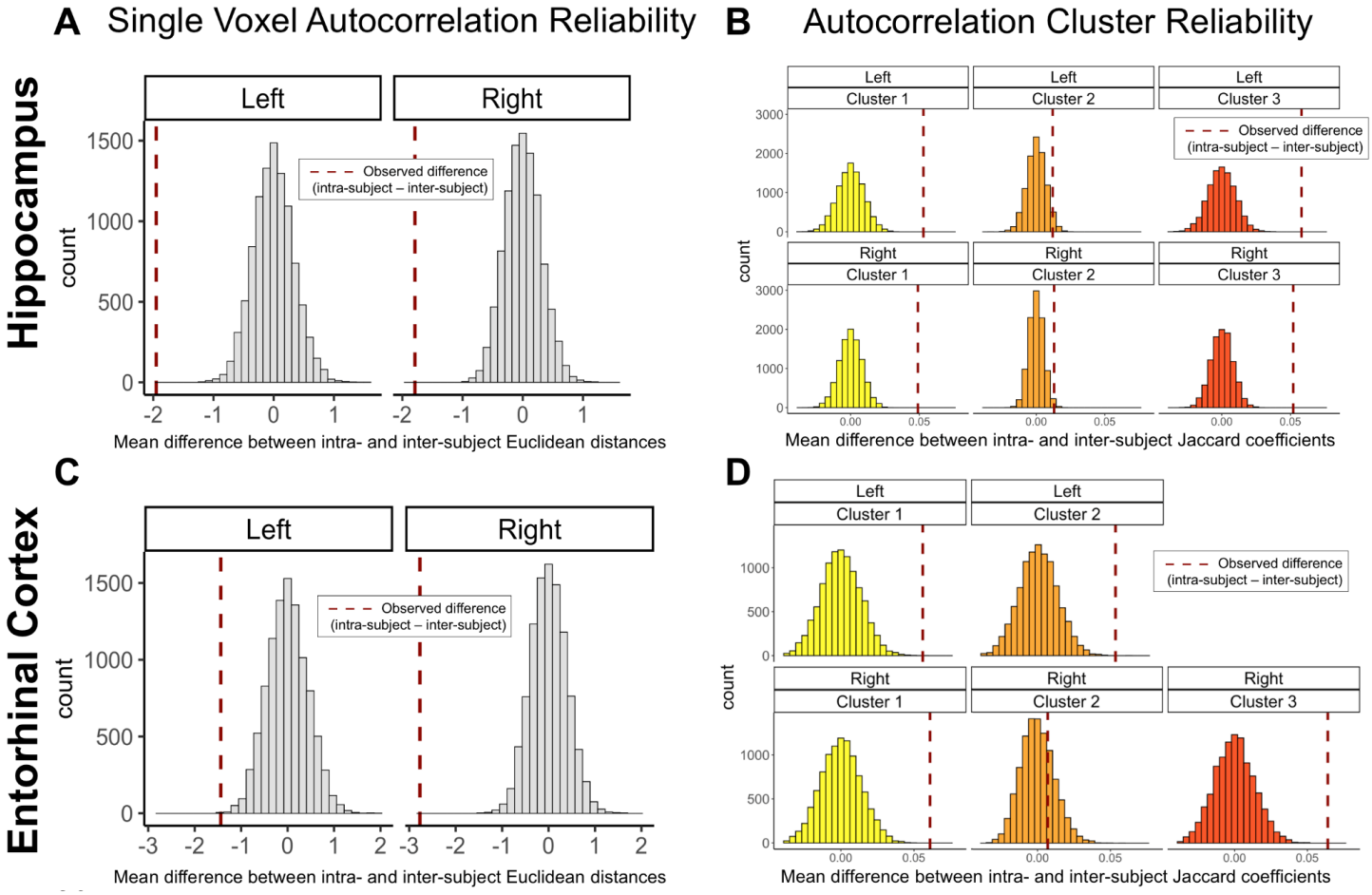

Figure 3. Hippocampal and Entorhinal cortex reliability measures. A,C) Single Voxel Autocorrelation Reliability. Distribution of shuffled and permuted mean difference of intra- and inter-subject Euclidean distances for the (A) hippocampus and (C) entorhinal cortex. Dashed lines represent the observed mean difference between intra- and inter-subject Euclidean distance. Significant negative values indicate that single voxel autocorrelation values were more similar within an individual than across individuals. **B, D) Autocorrelation Cluster Reliability.** Distribution of shuffled and permuted mean difference of intra- and inter-subject Jaccard coefficients for each cluster. Dashed lines represent the observed difference between intra- and inter-subject Jaccard coefficients for each cluster. (B) In both hemispheres of the hippocampus, Clusters 1 and 3 were more reliable within individuals compared to Cluster 2. (D) In the entorhinal cortex, Cluster 1 and Cluster 2 were reliable within individuals in the left hemisphere, whereas Cluster 1 and 3 were reliable within individuals in the right hemisphere.

Entorhinal cortex

Spatial distribution of single voxel autocorrelation

We repeated the analyses above in the ERC. To illustrate the distribution of autocorrelation values of individual voxels throughout the ERC, we plotted the group-level single voxel autocorrelation maps for lags 1-5 (Figure 4A). The maps illustrate a difference in single voxel autocorrelation throughout the ERC. Specifically, voxels with higher single voxel autocorrelation were mainly in the posterior-medial region whereas voxels with lower single voxel autocorrelation were mainly in the anterior-lateral region (in both left and right ERC).

Single voxel autocorrelation – Reliability results

Nonparametric permutation tests comparing intra-subject and inter-subject Euclidean distance revealed reliable results in both the left (intra-subject: 11.43 ± 3.64, inter-subject: 12.87 ± 2.83, $P < 0.001$ and right ERC (intra-subject: 10.41 ± 2.63, inter-subject: 13.19 ± 2.53, $P < 0.001$; Figure 3C). This analysis demonstrates the reliability of the single voxel autocorrelation and suggests that single voxel autocorrelation patterns between vectors generated from two runs of the *same* participant were more similar than two runs from *different* participants (lower intra-subject Euclidean distances compared to inter-subject Euclidean distances).

Autocorrelation Clustering

The group-level clustering analysis on the voxels within the ERC revealed two distinct clusters in the left hemisphere and three clusters in the right (Figure 4B). For comparison, cluster maps from two runs of an example participant are shown in Figure 4B. Cluster 1 was located in the posteromedial ERC and had the highest single voxel autocorrelation values in both left and right hemispheres. Cluster 2 was observed in the left hemisphere and was located towards the anterior-lateral ERC with low single voxel autocorrelation values. In the right hemisphere it was an intermediate cluster. Cluster 3 was only observed consistently in the right hemisphere and was located in the anterior-lateral ERC with the lowest single voxel autocorrelation values. We computed the group-level single voxel autocorrelation for each cluster and plotted it across all 5 lags (Figure 4D). Across all 5 lags, Cluster 1 consistently had the highest single voxel autocorrelation values, followed by Cluster 2 and Cluster 3.

Autocorrelation Clustering – Reliability results

The reliability measure for ERC clusters was calculated by the Jaccard coefficient (Figure 3D). Nonparametric permutation tests comparing intra-subject and inter-subject cluster overlap revealed reliable results in the left and right

hemisphere. In the left hemisphere, the Cluster 1 ($P < 0.001$) and Cluster 2 ($P < 0.001$) were reliable. In the right hemisphere, Cluster 1 ($P < 0.001$) and Cluster 3 ($P < 0.001$) were reliable. This suggests that these clusters were highly reliable within individuals. In the right hemisphere, Cluster 2 had very small Jaccard values, suggesting less reliability within individuals (Right: $P = 0.53$).

Gradients of single voxel autocorrelation (lag 1)

Single voxel autocorrelation values for lag 1 were projected onto X (medial-lateral), Y (posterior-anterior), and Z (inferior-superior) axes. As shown in Figure 4C, in every participant, single voxel autocorrelation values gradually decreased in the medial-to-lateral direction and the posterior-to-anterior direction (Figure 4C). We found a gradient of low-to-high autocorrelation along the inferior-superior axis, which is due to the fact that the posterior region of the ERC is more superior than its anterior region. We observed a gradient of cluster assignment that complemented the single voxel autocorrelation gradients, where high-to-low gradients were also associated with a cluster gradient from Cluster1 to Cluster 2.

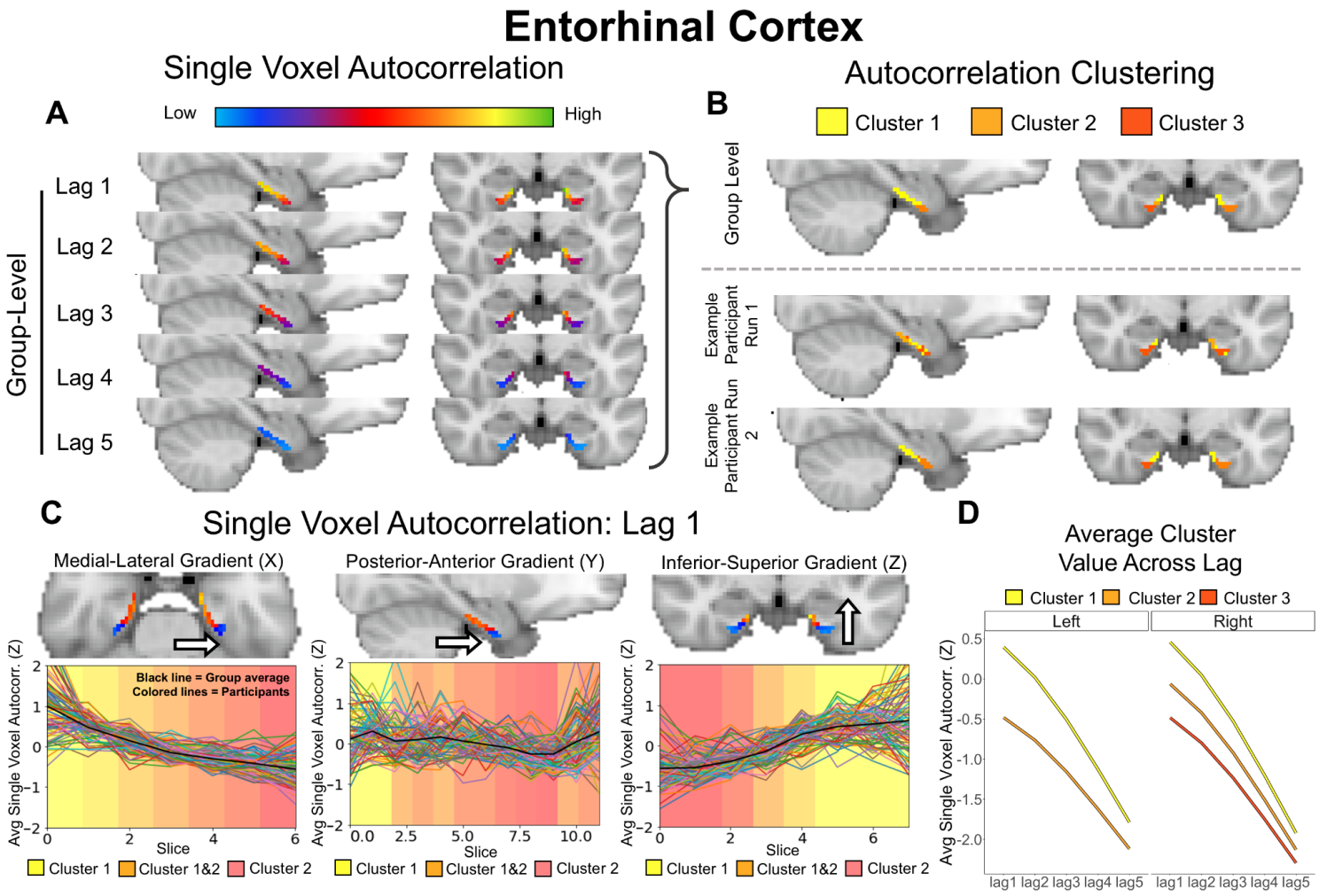

Figure 4. Entorhinal cortex. Single Voxel Autocorrelation. A) Group-level single voxel autocorrelation maps averaged across all runs for all participants. **Autocorrelation Clustering. B)** Group-level clusters (top) and run-level cluster maps for two runs from an example participant (bottom). Two distinct clusters were found in the left hemisphere and three in the right hemisphere. In the left hemisphere, Cluster 1 was located in the posterior-medial ERC and Cluster 2 was in the anterior-lateral ERC. In the right hemisphere Cluster 1 was located in the posterior-medial ERC, Cluster 3 was located in the anterior-lateral ERC, and Cluster 2 was located between Cluster 1 and 3. **C) Single Voxel Autocorrelation: Lag 1.** Single voxel autocorrelation projected below onto three axes (X, Y, and Z) to visualize changes in medial-lateral, anterior-posterior, and inferior-superior directions (for the left hemisphere; right hemisphere looked similar). The average cluster assignment of voxels on each slice is presented as the background color to show the gradation in values along the three axes (Note the gradation depicts only Cluster 1 and 2 as there were only two significant clusters found in the left hemisphere). **D) Average Cluster Value Across Lag.** Average group-level single voxel autocorrelation values for each cluster at each lag. In the left hemisphere, Cluster 1 was associated with the highest single voxel autocorrelation values and Cluster 2 with low autocorrelation values. In the right hemisphere, Cluster 1 was associated with the

highest single voxel autocorrelation, Cluster 2 with intermediate values, and Cluster 3 with the lowest. This was consistent across all 5 lags.

Dataset 2: Navigation *fMRI*

We next aimed to replicate the observed effects in task fMRI and relate changes in single voxel autocorrelation to behavior. Specifically, we were interested in how single voxel autocorrelation throughout the hippocampal long axis might be modulated by differences in difficulty during a temporally-extended navigation task. Therefore, we performed our single voxel autocorrelation analyses on a task fMRI dataset acquired while participants navigated in a familiar virtual reality environment (previously described in Brunec, Bellana et al., 2018). Here, 19 participants were scanned while navigating Google Street View routes around the city of Toronto. Participants navigated four different types of routes that varied in their navigational difficulty: GPS (unfamiliar routes guided by an arrow), Familiar (highly familiar routes), Unfamiliar (routes that were less familiar), and Mirrored (familiar routes that were left-right reversed). Participants completed four unique routes in each condition, sixteen routes in total (1 route = 1 scanned run). Due to the lower spatial resolution in this dataset we were not able to examine the ERC and, thus, these analyses focused only on the hippocampus.

Hippocampus

Spatial distribution of single voxel autocorrelation

To compute the single voxel autocorrelation, we completed the same procedure outlined in Dataset 1. In Dataset 2 the TR was 2000 ms; therefore, single voxel autocorrelation for 2 lags (or 2 TRs) was calculated. We observed a difference in single voxel autocorrelation along the anterior-posterior and medial-lateral hippocampal axes, where voxels with higher single voxel autocorrelation were found in the anterior-medial hippocampus and voxels with lower single voxel autocorrelation were found in the posterior-lateral hippocampus. Figure 5A shows the group-level single voxel autocorrelation maps for the four navigation conditions (as single voxel autocorrelation maps for lags 1-2 were similar, only lag 1 is depicted in Figure 5A). The spatial distribution of single voxel autocorrelation was similar across navigation conditions and was also similar to the findings from Dataset 1. In the next section, we investigate the differences between conditions in more depth.

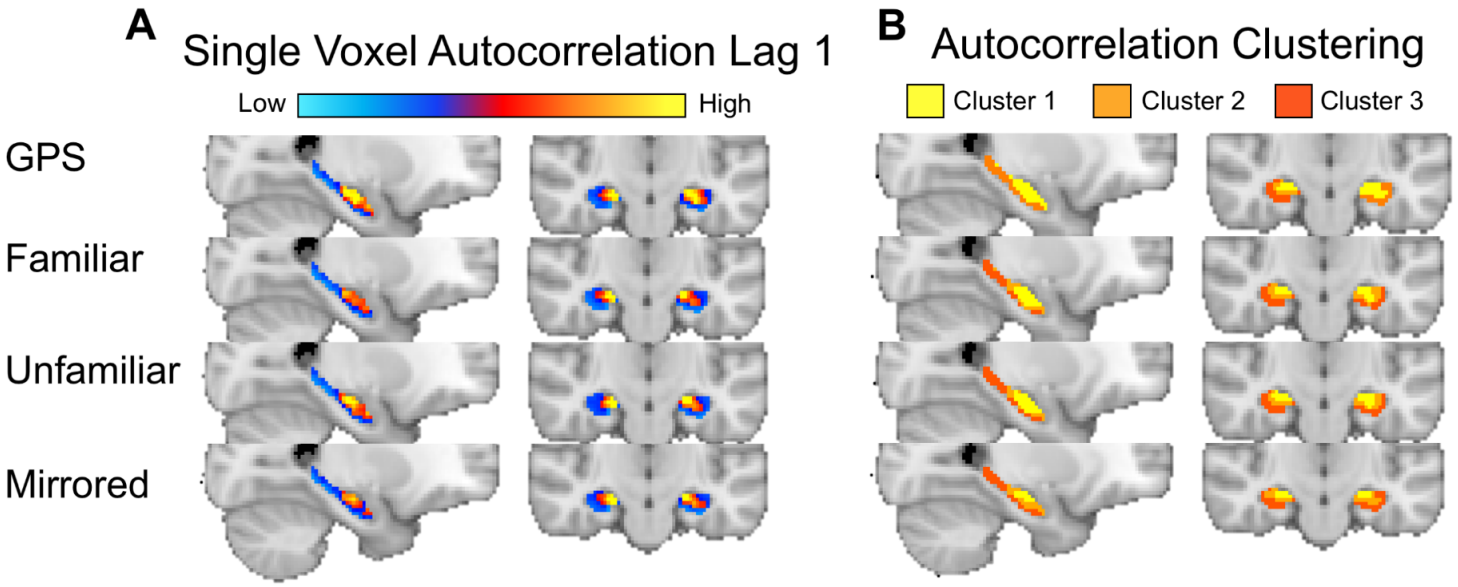

Figure 5. A) Single Voxel Autocorrelation: Lag 1. Single voxel autocorrelation values at lag 1 for every voxel in the hippocampus during spatial navigation. These values are averaged across run and participant for each of the GPS, Familiar, Unfamiliar and Mirrored conditions. A gradient from high to low autocorrelation is observed in the anterior-posterior and medial-lateral axes, across all navigation conditions. **B) Autocorrelation Clustering.** Cluster maps averaged across run and participant for each route type. High single voxel autocorrelation voxels cluster in the anterior-medial hippocampus and low single voxel autocorrelation voxels cluster in the posterior-lateral hippocampus.

Autocorrelation Clustering

In order to determine clusters of single voxel autocorrelation within each navigational condition, we repeated the autocorrelation clustering procedure described above in Dataset 1 within the hippocampus. As with Dataset 1, this revealed three distinct clusters in the left and right hemispheres for the Familiar, Unfamiliar and Mirrored conditions (Figure 5B). For Familiar, Unfamiliar, and Mirrored conditions, Cluster 1 was located in the anterior-medial HPC and had the highest single voxel autocorrelation. Cluster 3 was located in the posterior-lateral hippocampus and had the lowest single voxel autocorrelation. Cluster 2 was located between Cluster 1 and 3 and had intermediate single voxel autocorrelation. The GPS condition had three clusters in the right hemisphere and only two in the left.

Relating single voxel autocorrelation to navigation condition

Subjective difficulty ratings collected after each route (1 = difficult, 9 = easy) suggested that across the navigation conditions, navigational difficulty increased. Participants rated the GPS routes as the easiest (M = 7.2, SD = 1.46), followed

by the Familiar condition (M = 6.98, SD = 2.05), Unfamiliar condition (M = 4.35, SD = 2.66), and the Mirrored condition, which was subjectively the most difficult (M = 3.97, SD = 2.42).

As navigation becomes more difficult, it is beneficial to integrate or maintain information over time, which may be reflected in changes in single voxel autocorrelation. Specifically, more stable neural dynamics might enable individuals to maintain information as one moves towards a goal. This prediction leads to two possibilities. In the first, as navigational difficulty increases we might observe a uniform change in single voxel autocorrelation across all voxels in the hippocampus. A second possibility is that as difficulty increases, voxels that tend to exhibit high autocorrelation during rest would differentially increase their autocorrelation relative to voxels that tend to exhibit low autocorrelation. To investigate these possibilities, we calculated the slope of the single voxel autocorrelation (lag 1) along the anterior-posterior and medial-lateral axes. If navigational difficulty leads to a uniform increase in autocorrelation, we would observe no changes in the slope across these axes. However, if navigational difficulty disproportionately affects the regions of the hippocampus that show high autocorrelation during rest (Figure 2), then more difficult routes would elicit a larger difference in autocorrelation values along the anterior-posterior and medial-lateral axes, and therefore, a steeper slope. For easier routes, there would be less difference in autocorrelation along the two axes, suggesting more homogeneity of temporal dynamics along the axis and a shallower slope of autocorrelation.

Anterior-posterior HPC axis

Comparing single voxel autocorrelation slopes

We compared autocorrelation slopes in the four route conditions: GPS, Familiar, Unfamiliar, and Mirrored. For each participant, we averaged the single voxel autocorrelation (lag 1) across all voxels on each 3mm slice of the hippocampus (posterior-to-anterior direction) and calculated the slope coefficient across slices. In both the left and right hemisphere, across all four navigation conditions, the slope was positive, suggesting lower autocorrelation in the posterior hippocampus and higher autocorrelation in the anterior hippocampus, which is consistent with our findings from the clustering and single voxel autocorrelation lag 1 analyses. Across participants, Mirrored runs had steepest slopes (*Left:* M = 0.79, SD = 0.60; *Right:* M = 0.55, SD = 0.80) followed by Unfamiliar (*Left:* M = 0.69, SD = 0.53; *Right:* M = 0.41, SD =0.40), Familiar (*Left:* M = 0.63, SD = 0.46; *Right:* M = 0.31, SD = 0.25), and GPS routes (*Left:* M = 0.53, SD = 0.42; *Right:* M = 0.21, SD = 0.28).

To test whether there was a significant difference between single voxel autocorrelation during different navigation conditions, we ran a mixed effects model on the single voxel autocorrelation slopes along the anterior-posterior axis. We included hemisphere and condition (GPS, Familiar, Unfamiliar, and Mirrored) as predictors in the model and participants as a random intercept in the random effects term. We found a significant effect of hemisphere ($F(1, 481.99) = 42.22$, $p < .001$) and a significant effect of navigation condition ($F(3, 483.04) = 6.92$, $p < .001$) (Figure 6A). Their interaction was not significant.

A post hoc analysis of the main effect of hemisphere revealed that the single voxel autocorrelation slope was greater in the left hippocampus compared to the right hippocampus ($t(482) = 6.49$, $p < .001$). Pairwise comparisons of the different navigational conditions (collapsed across hemisphere) revealed that single voxel autocorrelation slopes were significantly greater for the Mirrored compared to GPS ($t(484) = 3.88$, $p < .001$) and Familiar ($t(482) = 3.71$, $p < .01$). There was no significant difference between Mirrored and Unfamiliar conditions. These results suggest that, across hemispheres, the single voxel autocorrelation slopes along the anterior-posterior axis were modulated by navigation difficulty: navigation runs with a steeper gradient of autocorrelation were related to more difficult navigation conditions. We compared the average single voxel autocorrelation at the two posterior-most and two anterior-most slices and found that single voxel autocorrelation was higher in the anterior hippocampus compared to the posterior hippocampus in both the left and right hemisphere (Left: anterior > posterior $t(1998) = 22.23$, $p < .001$; Right: anterior > posterior $t(1998) = 13.49$, $p < .001$). This finding suggests that increases in the autocorrelation slope along the anterior-posterior axis across conditions were driven by an increase in the anterior hippocampus.

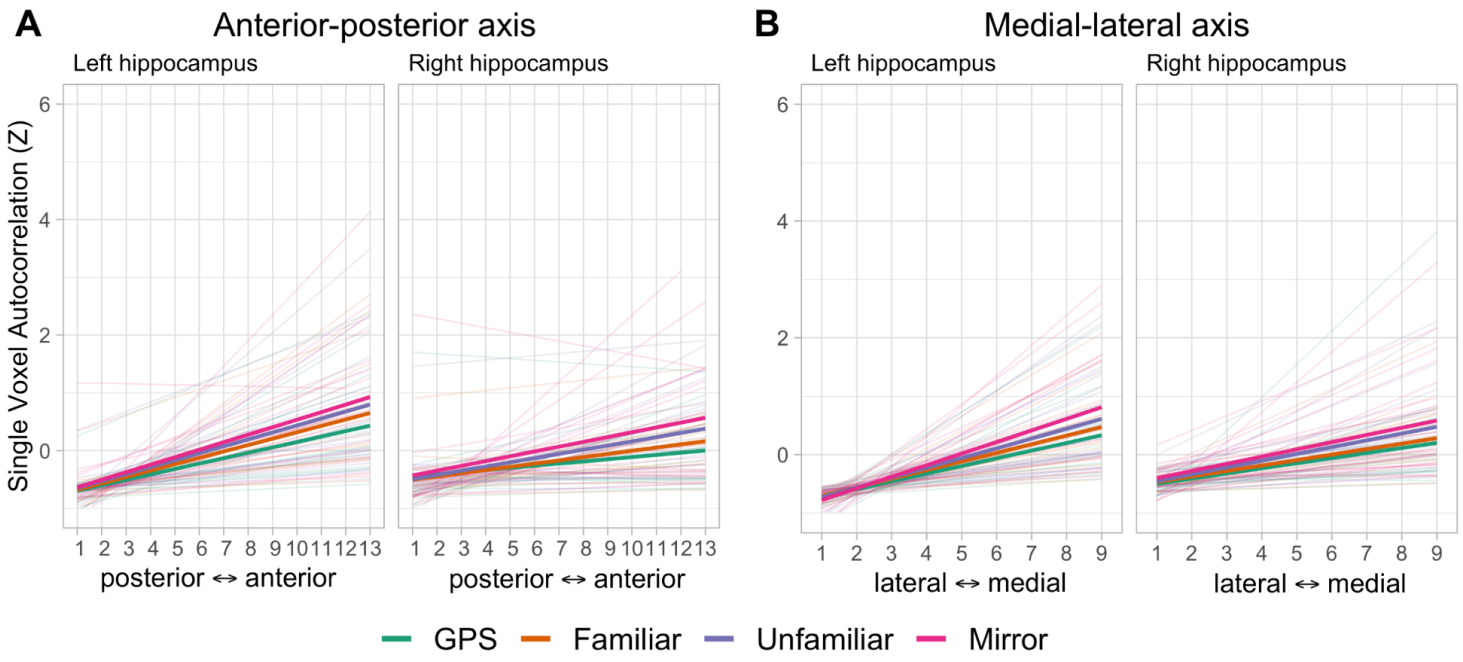

Figure 5. Effect of navigational condition on single voxel autocorrelation slopes. Average single voxel autocorrelation per slice along the anterior-posterior and medial-lateral axes for each navigation condition. **A) Anterior-posterior axis.** The left hippocampus had greater single voxel autocorrelation slopes compared to the right hippocampus. Across both hemispheres, slope along the anterior-posterior axis was modulated by navigational condition. The slope was greatest when participants navigated difficult routes (Mirrored and Unfamiliar routes) compared to easy routes (GPS and Familiar routes) **B) Medial-lateral axis.** The left hippocampus had greater single voxel autocorrelation slopes compared to the right hippocampus. Across both hemispheres, slope along the medial-lateral axis was modulated by navigational condition. The slope was greatest when participants navigated Mirrored routes compared to GPS, Familiar, and Unfamiliar routes. Bold lines represent the group average across all participants, faded lines represent each participant.

Medial-lateral HPC axis

Comparing single voxel autocorrelation slopes

For each participant, we averaged the single voxel autocorrelation (lag 1) across all voxels on each 3mm slice of the hippocampus (lateral-to-medial direction) and calculated the slope coefficient across slices. In both the left and right hemisphere, across all four navigation conditions, the slope was positive, suggesting lower autocorrelation in the lateral hippocampus and higher autocorrelation in the medial hippocampus. This observation is consistent with our findings from the clustering and single voxel autocorrelation lag 1 analyses. Across participants, Mirrored runs had steepest slopes (*Left:* M = 1.63, SD = 1.15; *Right:* M =1.45, SD = 1.77) followed by Unfamiliar (*Left:* M = 1.37, SD =

0.95; *Right:* M = 1.13, SD = 1.20), Familiar (*Left:* M = 1.21, SD = 0.74; *Right*: M = 0.92, SD = 0.98), and GPS routes (*Left:* M =1.08, SD = 0.80; *Right:* M = 0.89, SD = 1.45).

We ran a mixed effects model on the single voxel autocorrelation slopes along the medial-lateral axis with hemisphere and condition as predictors and participant as a random intercept in the random effects term. We found a significant effect of hemisphere ($F(1, 482.03) = 5.03$, $p < .05$) and a significant effect of navigation condition ($F(3, 482.71) = 7.10$, $p < .001$) (Figure 6B). Their interaction was not significant.

A post hoc analysis of the main effect of hemisphere revealed that the single voxel autocorrelation slopes were greater in the left than the right hippocampus ($t(482) = 2.24$, $p < 0.05$). Pairwise comparisons of the different navigational conditions (collapsed across hemisphere) revealed that single voxel autocorrelation slopes were significantly greater for the Mirrored compared to GPS ($t(483) = 3.42$, $p < .01$), greater for Mirrored compared to Familiar ($t(482) = 4.18$, $p < .001$), and greater for Mirrored compared to Unfamiliar ($t(482) = 2.61$, $p < .05$). These results suggest that, across hemispheres, the single voxel autocorrelation slopes along the medial-lateral axis were modulated by navigation difficulty: navigation runs that had a steeper gradient of autocorrelation were related to more difficult navigation conditions. We compared the average single voxel autocorrelation at the two medial-most and two lateral-most slices and found that single voxel autocorrelation was higher in the medial hippocampus than the lateral hippocampus in both the left and right hemisphere (Left: medial > lateral $t(1998) = 17.76$, $p < .001$; Right: medial > lateral $t(1998) = 14.91$, $p < .001$). This suggests that increases in the autocorrelation slope along the medial-lateral axis across conditions is driven by an increase in the medial hippocampus.

Discussion

Here we present a novel autocorrelation measure to investigate intra-hippocampal and intra-entorhinal processing. We provide the first evidence of a medial-lateral gradient of autocorrelation in the hippocampus, as well as a posterior-medial and anterior-lateral gradient in the ERC. We found that voxels in the anterior-medial hippocampus have a highly correlated, slower changing signal, whereas voxels in the posterior-lateral hippocampus have a less correlated, faster changing signal (Figure 2) (Brunec, Bellana, et al., 2018; Raut et al., 2020). Our study highlights the importance of examining the medial-lateral

axis of the hippocampus, which has previously been an under-studied feature of hippocampal organization. We find novel evidence for a continuous gradient in the ERC, with greater autocorrelation in the posteromedial ERC and lower autocorrelation in the anterolateral ERC (Figure 4). Lastly, the present study is the first to show that gradients of single voxel autocorrelation in the hippocampus are related to behavior during navigation. Specifically, autocorrelation gradients in the anterior-posterior and medial-lateral axes, as measured by the slope, increased for difficult routes and were steepest in the left hemisphere (Figure 6). This increase in slope was driven by increases in the anterior-medial hippocampus.

Our data-driven approach — which allows voxels to cluster according to their single voxel autocorrelation, uncovered a multidimensional gradient in both the anterior-posterior and medial-lateral axes in both the hippocampus and ERC (Figure 2 & 4). In the hippocampus, the anterior-posterior axis has been studied with respect to its role in representing graded information, for example coarse-grained to fine-grained information (Poppenk et al. 2013; Strange et al., 2014), large to small spatial distances (Evensmoen et al., 2013; Nielson et al., 2015; Peer et al., 2019;) and long to short temporal distance (Bellmund et al., 2019; Nielson et al., 2015). Investigations of representational differences along the medial-lateral axis, however, have been limited because prior work has used predefined anatomical segmentations limited to the anterior and posterior portions of the long axis of the hippocampus. Our single voxel autocorrelation method is not restricted by predefined ROIs and proves to be a more precise measure that detects subtle differences in signal along the medial-lateral axis that have been previously overlooked and that are modulated by navigational difficulty. In addition to the hippocampus, we found similar distinctions in the ERC. We observed a gradient of single voxel autocorrelation organization, such that greater single voxel autocorrelation was observed in the posterior-medial region and lower single voxel autocorrelation in the anterolateral region of the ERC (Figure 4). This gradient is consistent with previous neuroimaging investigations of ERC which used high-resolution fMRI and functional connectivity to define distinct subregions within the human ERC (Maass et al., 2015; Navarro Schröder et al., 2015). Our analytic technique, however, goes beyond this prior work by demonstrating, for the first time, continuous gradients of autocorrelation in the ERC.

The present study demonstrates that the autocorrelation of the fMRI signal is not just global noise, but instead carries meaningful information about brain function that is directly related to behavior. Autocorrelation is frequently characterized as

noise that masks meaningful signals and is unrelated to cognition, but recent research suggests that autocorrelation might be a global organizing principle and reflects intrinsic functional hierarchies in the brain (Irish & Vatansever, 2020; Raut et al., 2020). For example, an analysis of resting state fMRI data calculated the autocorrelation decay in single voxels across a temporal window (0-8 seconds) and found a significant large-to-small timescale gradient along the anterior-posterior axis in the hippocampus (Raut et al., 2020), which is consistent with reports by Brunec, Bellana, et al. (2018). Recent research has also linked autocorrelation with global differences in cognitive state (task vs. rest) and mental state (healthy vs. schizophrenia) (Arbabshirani et al., 2019). While this study cannot address the direct link between the autocorrelation gradients and behavior, this work suggests that autocorrelation can be used to discriminate between cognitive states that are uniform across the brain, leaving open the question of how autocorrelation gradients in specific brain regions might be related to differences in cognition during a behavioral task. Our analysis technique demonstrated novel gradients during resting state, and can also be applied to task related activation to reveal their relation to on-going behavior and is the first to show that changes in single voxel autocorrelation gradients are directly related to changes in difficulty during a navigation task.

Anterior hippocampal voxels are more stable across time compared to the posterior hippocampus, which might enable the anterior hippocampus to maintain prior information across time during goal-directed navigation (Brunec, Bellana, et al., 2018). Our method proved to be a more sensitive measure than previous techniques (e.g., Brunec, Bellana et al., 2018) because we were able to show differences in autocorrelation across navigation conditions. More specifically we found that the autocorrelation in the anterior-medial hippocampus increased during navigation of difficult routes (Figure 6). The autocorrelation signal may reflect the mechanism by which the hippocampus holds onto the past and carries it forward during navigation when we are in unfamiliar or unpredictable environments. For example, when navigating an unfamiliar route to a distant goal, the local details of the environment might not be helpful to orient oneself in relation to the goal; it may be more efficient, therefore, to keep in mind a coarser, overall map of the environment with information about steps already taken in order to reach the goal destination successfully. This large-scale representation may not be as useful to keep online during navigation of well-known or familiar routes where local details are sufficient for orienting and navigating to the goal, which could explain the decreased single voxel autocorrelation in the signal throughout the familiar routes (Figure 6). This hypothesis is supported by previous research which has shown that the anterior hippocampus plays an

important role in representing larger spatial and temporal distances (Evensmoen et al., 2013; Nielson et al., 2015) as well as representing coarser-grained, global representations (Collin et al., 2015).

We found that both of the single voxel autocorrelation gradients (anterior-posterior and medial-lateral) were steeper in the left hemisphere compared to the right. It is still unclear whether this is representative of a stable difference in autocorrelation between the hemispheres or whether this reflects different types of information that are engaged across the two hemispheres during navigation. Future research is needed to determine the nature of this hemispheric difference.

Another non-mutually exclusive possibility is that the single voxel autocorrelation is representative of predictions that are cast into the future. The notion that increased temporal similarity is indicative of an extended spatiotemporal representation is supported by recent work investigating the predictive horizons along the hippocampal anteroposterior axis during navigation (Bruenc & Momennejad, 2019). Brunec and Momennejad (2019) found that as participants virtually navigated familiar, real-world routes (a subset of the familiar routes presented here), hippocampal activity was related to a hierarchical scale of horizon representations, in which the posterior hippocampus represented steps closer in the future trajectory (~25m) while the anterior hippocampus represented steps further in the future trajectory (~175m). It is possible, therefore, that the single voxel autocorrelation we observed helps represent an upcoming navigational trajectory, with immediate goals represented in posterior-lateral regions and more distal goals in the anterior-medial hippocampus. The predictive role of the hippocampus has also been observed in perception, particularly when the stimulus was visually complex (Kok et al., 2020). Our method and findings open the door for future studies using high resolution neuroimaging in combination with a task that parametrically modulates the amount of information that is carried over time in both predictable (familiar) and unpredictable (unfamiliar) environments to uncover content that is carried forward via the autocorrelation signal.

Although we were not able to relate the autocorrelation in ERC to behavior due to the resolution of the navigation data, if we apply the same logic we used for the hippocampus, our findings are consistent with the notion that alERC codes for local details and perceptual aspects of experience, whereas the pmERC codes for global contexts. Specifically, the (antero-)lateral ERC has been linked to fine-grained temporal processing (Montchal et al., 2019; Tsao et al., 2018) and to processing of object-context and within-object details (Yeung et al., 2017; 2019).

The low autocorrelation we observed in the alERC might indicate faster updating of moment-to-moment changes and therefore support fine-grained representations. Future investigations can use our method to analyze continuous changes along both anterior-posterior and medial-lateral axes of the ERC without being restricted to anatomical subfield segmentations, perhaps revealing a more nuanced understanding of the organization of the ERC. We observed two consistent clusters in the left hemisphere and three consistent clusters in the right hemisphere, which suggests that in this dataset there was more variability in the left ERC intermediate cluster. Future research is needed to determine whether this is a stable property of the temporal organization of the left ERC that can be replicated across other datasets.

It is currently unclear how the posterior-medial and anterior-lateral subregions of the ERC are functionally related to the anterior and posterior regions of the hippocampus. In the present study we found that clusters in the anterior-medial hippocampus and posterior-medial ERC had high single voxel autocorrelation, whereas clusters in the posterior-lateral hippocampus and antero-lateral ERC had low single voxel autocorrelation. These distinctions along the anterior-posterior and medial-lateral axes of the ERC are consistent with previous functional connectivity findings (Navarro Schröder et al., 2015), however functional connectivity and neuroanatomical studies in humans have been limited and do not find any clear differences between the anterior and posterior portions of the hippocampus with respect to their connectivity to different subregions in the ERC (Maass et al., 2015; Navarro Schröder et al., 2015). Functional connections between these regions might be evident in the scale of information processing in the hippocampus and ERC. For example, it is possible that the pattern of low single voxel autocorrelation in anterior-lateral ERC and posterior-lateral hippocampus supports fine-grained processing — precise temporal processing in the anterior-lateral ERC (Bellmund et al., 2019; Montchal et al., 2019) and local spatial details in the posterior hippocampus (Doeller et al., 2008; Evensmoen et al., 2013; Hirshhorn et al. 2012; Lee et al., 2012).

There are currently no clear neuroanatomical links between the anterior-lateral ERC and posterior-lateral hippocampus or the anterior-medial hippocampus and posterior-medial ERC. There are, however, probable connections between the anterior ERC and lateral hippocampus and posterior ERC with medial hippocampus (Strange et al., 2014; Witter & Amaral 2020; Nilssen et al., 2019; Witter et al., 2017). Our results, therefore, open the door for future investigations to characterize more fully the nature of anterior and posterior hippocampal signal dynamics in relation to the entorhinal subregions in humans and in relation to

other structures, such as prefrontal cortex (Barredo et al., 2015; Vaidya & Badre, 2020).

The results presented here reveal, for the first time, two continuous gradients along the anterior-posterior and medial-lateral axes in the hippocampus and ERC. One outstanding question is whether there is new information that can be gained by investigating the two autocorrelation gradients separately, or whether the information they represent is redundant. For example, do tasks that evoke a steep autocorrelation gradient along the anterior-posterior axis necessarily evoke a similarly steep gradient along the medial-lateral axis or are there tasks in which these two gradients act in opposing directions (e.g., change in anterior-posterior slope but no change or change in opposite direction in medial-lateral slope). Another outstanding question is whether our novel single voxel autocorrelation method can be applied with shorter timescales so that they can be used with event-related designs. Here we use the entire timecourse of the voxel's activity to calculate the single voxel autocorrelation throughout the entire run, but it remains to be seen whether we can adapt our method to examine how autocorrelation changes over shorter time windows. This would allow us to ask new questions about what kind of information is being carried in the autocorrelation signal during discrete or shorter events and at event boundaries, which are known to trigger changes in hippocampal activity associated with integration of information across events (Dubrow & Davachi, 2013; Ezzyat & Davachi, 2014). Finally, this method can be used to investigate differences in autocorrelation within subfields of the hippocampus. For example, it has been proposed that CA1 is implicated in integrating information in memory, whereas DG/CA3 which mediates pattern separation may be more implicated in making fine distinctions in memory (Kyle et al., 2015; Leutgeb et al., 2004; Schapiro et al., 2017; Yassa & Stark, 2011). Integration processes in CA1, therefore, might be supported by voxels with high single voxel autocorrelation while separation processes in DG/CA3 might be better supported by low single voxel autocorrelation. Future research using our method and high-resolution fMRI is needed to test these differences within subfields.

Our studies were inspired initially by single-unit recording studies in rodents (Brun et al., 2008; Cavanagh et al., 2016; Gothard et al.,1996; Kjelstrup et al., 2008; Maurer et al., 2005). We believe our findings, however, have gone beyond replicating the rodent findings in humans, a worthy task in its own right, but extended the findings to the point that they can now be used to inform future studies in rodents and humans. We provide some examples in which this is the case. For example, our method enabled us to find differences in autocorrelation

along the anterior-posterior and medial-lateral axes in the entorhinal cortex, which have only been examined in a restricted region in rodents (Brun et al., 2008). Our findings are consistent with neuroanatomical and neurophysiological divisions in that structure (human: Maass et al., 2015; monkey: Witter & Amaral, 2021; rat: Witter et al., 2017). Second, although activity of a single voxel, comprised of thousands of neurons, may be considered to be a coarser unit of analysis than recordings from single units, it may be the case that it is the operation of a population of these neurons that is most closely linked to organizational temporal dynamics. It is the gradients revealed by autocorrelation at the single voxel level that enabled us to link hippocampal dynamics to behavior. In addition, we were able to segment the populations into clusters, suggesting subdivisions that would not be evident at the single-unit level. It would be worthwhile to determine whether similar clusters are found in rodents and examine their functional significance. Similar analyses at the population-level in rodents may yield information about the relation of neural dynamics to higher-level memory representations and goals, an enterprise that is just beginning (Jacob & Josselyn, 2020; Morrissey et al., 2017).

Our results provide compelling evidence for a gradation of single voxel autocorrelation in the hippocampus and ERC. As predicted, our single voxel method proved to be a fine-grained measure that revealed subtleties in the spatial organization of autocorrelation, going beyond prior methods, and allowed us to observe graded signals along anterior-posterior and medial-lateral axes in both regions. Further, we show for the first time that differences in single voxel autocorrelation gradients in the hippocampus can be directly related to differences in difficulty during a virtual navigation task, thus opening the door for future research to ask new questions of the autocorrelation signal and uncover how it is related to behavior.

Materials and Methods

Dataset 1: Resting state fMRI

Participants

We analyzed resting state fMRI data from 44 participants (14 male) from the Human Connectome Project (HCP) Retest dataset. This dataset consists of data from 44 participants who were scanned twice using the full HCP imaging protocol. All subject recruitment procedures and informed consent forms, including consent to share de-identified data, were approved by the Washington University Institutional Review Board (IRB) (Glasser et al. 2016). The present analysis of this dataset was approved by the University of Toronto research

ethics board.

Scanning parameters and preprocessing

Resting state data were collected using a multiband EPI pulse sequence (TR = 720 ms, TE = 33.1 ms, 72 slices with 2 mm thickness, FOV = 208 x 180 mm, voxel size = 2x2 mm, Flip angle = 52, Multiband factor = 8, Scan time = 14 minutes and 33 seconds). Each run was repeated twice, with a left-to-right and a right-to-left phase encoding direction. The presented results are generated from data with the left-to-right phase encoding direction.

Initial fMRI preprocessing steps already applied to the downloaded data included fieldmap correction, motion correction, brain extraction, registration to standard space, and intensity normalization (Glasser et al., 2013; Smith et al., 2013; Van Essen et al., 2013). The data were further preprocessed using the FIX tool in FSL (Griffanti et al., 2014; Salimi-Khorshidi et al., 2014), and noise components related to head motion and other artifacts were removed. To eliminate high frequency noise and artifacts, fMRI signals are low-pass filtered using MATLAB IIR Butterworth filter (designfilt function in Signal Processing Toolbox) with cutoff frequency of 0.1 Hz.

Single voxel autocorrelation method

Computing single voxel autocorrelation

Bilateral hippocampal and entorhinal masks were generated using the Harvard-Oxford Atlas in FSL. For each voxel inside each of the regions of interest (ROIs), unbiased autocorrelation (as implemented in MATLAB xcorr function) was calculated. Specifically, the timecourse of a single voxel's activity was correlated with itself shifted by a temporal lag, the length of 1 TR (Dataset 1 TR = 720 ms). We repeated this process, shifting the timecourse forward by 1 lag (720 ms) and correlating it with the original, non-shifted timecourse until a maximum temporal shift of 4 seconds was reached. We chose 4 seconds because it has been shown that the autocorrelation of the fMRI signal in the gray matter drops off after 4 seconds (i.e., it is not distinguishable from the autocorrelation of other noise) (Bollmann et al., 2018). For example, the non-shifted timecourse was correlated with lag 1 (length of 1 TR), lag2 (length of 2 TRs), etc. (Figure 1). The autocorrelation (AC) computed for each lag was stored in a vector. The autocorrelation vector (single voxel autocorrelation vector) contained 5 values (one single voxel autocorrelation for each lag). This approach resulted in a single voxel autocorrelation vector for each voxel (Figure 1A). All single voxel autocorrelation values were normalized by subtracting the mean and dividing by the standard deviation within each mask so that meaningful comparisons could

be made between the two fMRI datasets (resting state and task). Single voxel autocorrelation maps were then averaged across the first and second runs from the 44 participants to generate an average overall map (e.g., Figure 1B).

Single voxel autocorrelation – Reliability Analysis

To verify that the observed single voxel autocorrelation pattern was not a measurement artifact (e.g., head motion, magnetic field inhomogeneity, physiological artifacts, etc.), we tested the reliability of the single voxel autocorrelation pattern within an individual. In our case, the single voxel autocorrelation pattern was deemed reliable if there was a high degree of agreement between the single voxel autocorrelation values generated from different runs from the same participant compared to runs from different participants. Reliability of the single voxel autocorrelation values was measured by calculating the Euclidean distance (ED) between the single voxel autocorrelation vectors for all pairs of run-wise datasets. 44 participants with 2 repeated sessions produced 44 intra-subject and 3784 inter-subject ED values. The lower the ED between two single voxel autocorrelation vectors, the higher the similarity between them. We expected to see more similar single voxel autocorrelation patterns between single voxel autocorrelation vectors generated from two runs of the same participant compared to two runs from different participants (lower intra-subject ED compared to inter-subject ED). The inter-subject and intra-subject ED are not completely independent from one another, therefore we used nonparametric permutation to test for significance. We randomly shuffled the intra-and inter-subject labels and pulled two samples of size 44 (intra-subject) and 3784 (inter-subject). We calculated the mean difference between the two samples and repeated this process 10,000 times, resulting in a histogram of mean differences under the null hypothesis (i.e., the difference between intra- and -inter-subject ED equal to zero). We compared the observed difference between intra- and inter-subject EDs with the null distribution and calculated nonparametric p-values. Permutation tests were conducted using a permutation testing package in Matlab (Laurens, 2021).

Computing single voxel autocorrelation clusters (Autocorrelation Clustering)

The Euclidean distance between the single voxel autocorrelation vectors of each voxel pair in each mask was calculated to create a distance matrix. The distance matrix was first normalized (i.e., divided by the maximum value) and then subtracted from 1 to generate a similarity matrix ranging from 0 to 1. This similarity matrix was used to generate hippocampal clusters using the modularity optimization algorithm proposed by (Blondel et al., 2008; Wickramaarachchi et al., 2014). Unlike the majority of the clustering methods, modularity optimization

does not require to assign the number of clusters and estimates the optimum number of clusters from data. In addition to clustering at the level of each individual, group-level clustering was performed by averaging the similarity matrices of all participants (e.g., Figure 1C).

Autocorrelation Clustering – Reliability Analysis

Reliability of the clustering was measured by calculating the overlap between the generated clusters using the Jaccard coefficient. The Jaccard coefficient of regions A and B is defined as:

$$J(A,B) = \frac{|A \cap B|}{|A \cup B|}$$

Where $|A \cap B|$ is the number of common voxels in both A and B (intersection) and $|A \cup B|$ is the number of voxels in A and B combined (union). Individual parcellations were then compared to the group-level parcellation to examine the consistency of parcellation. The Jaccard coefficient was calculated both intra-subject (overlap between clusters extracted from two runs from the *n*th subject) and inter-subject (overlap between the cluster from the *n*th subject and the same cluster estimated in all other subjects).

Assuming that the single voxel autocorrelation pattern is consistent across the two runs of the same participant, we expected there to be greater spatial overlap (higher Jaccard coefficient) among clusters within an individual compared to between different individuals. The Jaccard coefficients for clusters within participants are not completely independent from the Jaccard coefficients for clusters between participants, therefore we used nonparametric permutation to test for significance. For each cluster, we randomly shuffled the intra-and inter-subject labels and pulled two samples of size 44 (intra-subject) and 3784 (inter-subject). We calculated the mean difference between the two samples and repeated this process 10,000 times, resulting in a histogram of the mean differences under the null hypothesis (i.e., the difference between intra- and -inter-subject Jaccard coefficient equal to zero). We compared the observed difference between intra- and inter-subject Jaccard coefficients with the null distribution and calculated nonparametric P values.

Dataset 2: Navigation *fMRI*

Participants

Task fMRI data is from Brunec, Bellana, et al. (2018), where 19 participants (9 males; mean age 22.58 years, range 19-30 years) were scanned while navigating Google Street View routes around the city of Toronto. All subject

recruitment procedures and informed consent was approved by the University of Toronto research ethics board.

Paradigm

Participants met with the experimenter ahead of time and built routes that were either highly familiar or less familiar to them (e.g., frequently travelled or not). Participants then returned to the lab for their second session and were scanned while they navigated four different types of routes. 1) Familiar: participants started at a familiar landmark and navigated to a familiar goal destination via a familiar route, 2) Mirrored: participants started at a familiar landmark and travelled to a familiar destination via a familiar route, but the images of the route were mirrored (left-right reversed), 3) Unfamiliar: participants started at a familiar location, navigated to a familiar destination, but they were instructed to take an unfamiliar route between the two, and 4) GPS: participants started at an unfamiliar location in an unfamiliar part of town and pressed arrow keys following the directions displayed by an arrow on the screen to the goal destination. Participants completed four unique routes in each condition, sixteen routes in total (1 route = 1 scanned run). At the end of each route, participants rated the difficulty of the route on a scale from 1 (difficult) to 9 (easy).

Scanning parameters and preprocessing

Participants were scanned with a 3T Siemens MRI scanner at Baycrest's Rotman Research Institute. A high-resolution 3D MPRAGE T1-weighted pulse sequence image (160 axial slices, 1 mm thick, FOV = 256 mm) was first obtained to register functional maps against brain anatomy. Functional imaging was performed to measure brain activation by means of the blood oxygenation level dependent (BOLD) effect. Functional T2*-weighted images were acquired using echo-planar imaging (30 axial slices, 5 mm thick, TR = 2000 ms, TE = 30 ms, flip angle = 70 degrees, FOV = 200 mm). The native EPI resolution was 64 x 64 with a voxel size of 3.5mm x 3.5mm x 5.0mm. Images were first corrected for head motion using the Analysis of Functional NeuroImages (AFNI; Cox, 1996). All subsequent analysis steps were conducted using the statistical parametric mapping software SPM12.

Preprocessing involved slice timing correction, spatial realignment and co-registration, with a resampled voxel size of 3mm isotropic, with no spatial smoothing. As all of our analyses rely on covariance, we additionally regressed out the mean time-courses from participant-specific white matter, and cerebrospinal fluid masks, alongside estimates of the 6 rigid body motion parameters from each EPI run. To further correct for the effects of motion which

may persist despite standard processing (Power et al., 2012), an additional motion scrubbing procedure was added to the end of our preprocessing pipeline. Using a conservative multivariate technique, time points that were outliers in both the six rigid-body motion parameter estimates and BOLD signal were removed, and outlying BOLD signal was replaced by interpolating across neighboring data points. Motion scrubbing further minimizes any effects of motion-induced spikes on the BOLD signal, over and beyond standard motion regression, without leaving sharp discontinuities due to the removal of outlier volumes (for details, see Campbell et al., 2013). To enable comparisons at the group-level, the final step of the preprocessing involved warping participants' functional data to the MNI-space template.

Single voxel autocorrelation method

Computing single voxel autocorrelation

To compute the single voxel autocorrelation, we completed the same procedure outlined in Dataset 1. We used the same bilateral hippocampal masks to extract the HPC voxels in Dataset 2. For each voxel, the single voxel autocorrelation was calculated by repeatedly shifting temporal lags (length of 1 TR) until a maximum lag of 4 seconds was reached. In Dataset 2 the TR was 2000 ms; therefore, single voxel autocorrelation for 2 lags (or 2 TRs) was calculated, resulting in a maximum lag of 4 seconds. As outlined in the procedure above, single voxel autocorrelation values were normalized by subtracting the mean and dividing by the standard deviation. Single voxel autocorrelation was calculated for all four runs of each navigational condition (Familiar, Unfamiliar, Mirrored, GPS). The single voxel autocorrelation was averaged across the four scanned runs (unique routes), resulting in four different maps (one for each navigational condition). Single voxel autocorrelation maps were then averaged across the 19 participants to generate an average group map for each navigation condition.

Participants completed 16 navigation runs (four in each condition) at their own pace. Because the conditions varied in difficulty, the average number of TRs differed across conditions and participants. Every route was 2-10 km long and the average run (route) length was 137.6 TRs (2 s TRs). The average number of TRs was lowest in the GPS condition (M = 92.13, SD = 17.44), followed by the Familiar condition (M = 136.45, SD = 39.18), the Mirrored condition (M = 155.73, SD = 36.84), and the Unfamiliar condition (M = 158.78, SD = 32.13). In order to compare single voxel autocorrelation across scanned runs with a similar number of TRs/lengths, we chose to filter out any runs that were unusually short (that the participant either didn't complete or completed very quickly). We excluded runs that were less than 88 TRs long. This resulted in an average of 13.36 runs (SD =

1.21) per participant. The GPS runs were disproportionately shorter than the other conditions, resulting in more GPS runs excluded than other conditions. The average number of routes included in the following analyses per participant are as follows: Mirrored (M=3.89, SD=0.31), Unfamiliar (M=3.84, SD=0.50), Familiar (M=3.68, SD=0.47), GPS (M=1.95, SD=1.22).

Computing autocorrelation clusters (Autocorrelation Clustering)

We repeated the single voxel autocorrelation clustering procedure described above in Dataset 1 to determine clusters of single voxel autocorrelation within each navigational condition.

Relating single voxel autocorrelation to navigation condition

Calculating single voxel autocorrelation slopes

To investigate how the spatial distribution of single voxel autocorrelation is related to navigation difficulty, we compared the single voxel autocorrelation (lag 1) slopes across the four different conditions: GPS, Familiar, Unfamiliar, and Mirrored. First, for each participant, we extracted the single voxel autocorrelation (lag 1) from every voxel. We averaged the single voxel autocorrelation across all voxels on each slice of the hippocampus. We used 3 mm slices in the anterior-posterior direction (Y-direction), resulting in thirteen slices. Using a linear regression, we calculated the slope coefficient for the single voxel autocorrelation across slices for each navigation run. We then repeated the same procedure, using 3 mm slices in the medial-lateral direction (X-direction), resulting in 9 slices. We computed the slopes and compared them across navigation conditions and hemispheres.

To test whether there was a significant difference between single voxel autocorrelation during different navigation conditions, we ran a mixed effects model on the single voxel autocorrelation slopes along the anterior-posterior and medial-lateral axes. This analysis was conducted in R (R Core Team, 2019) using the afex (Singmann et al., 2020) and the tidyverse packages (Wickham, 2017).

References

Arbabshirani, M. R., Damaraju, E., Phlypo, R., Plis, S., Allen, E., Ma, S., Mathalon, D., ... & Calhoun, V. D. (2014). Impact of autocorrelation on functional connectivity. *NeuroImage, 102*(part2), 294–308. https://doi.org/10.1016/j.neuroimage.2014.07.045

Arbabshirani, M. R., Preda, A., Vaidya, J. G., Potkin, S. G., Pearlson, G., Voyvodic, J., ... & Calhoun, V. D. (2019). Autoconnectivity: A new perspective on human brain function. *Journal of neuroscience methods*, *323*(15), 68-76. https://doi.org/10.1016/j.jneumeth.2019.03.015

Barredo, J., Öztekin, I., & Badre, D. (2015). Ventral fronto-temporal pathway supporting cognitive control of episodic memory retrieval. *Cerebral Cortex*, *25*(4), 1004-1019.

Bellmund, J. L., Deuker, L., & Doeller, C. F. (2019). Mapping sequence structure in the human lateral entorhinal cortex. *Elife*, *8*, e45333. https://doi.org/10.7554/eLife.45333

Bellmund, J. L., Deuker, L., Schröder, T. N., & Doeller, C. F. (2016). Grid-cell representations in mental simulation. *Elife*, 5, e17089. https://doi.org/10.7554/eLife.17089

Berron, D., Neumann, K., Maass, A., Schütze, H., Fliessbach, K., Kiven, V., ... & Düzel, E. (2018). Age-related functional changes in domain-specific medial temporal lobe pathways. *Neurobiology of Aging*, *65*, 86-97. https://doi.org/10.1016/j.neurobiolaging.2017.12.030

Blondel, V. D., Guillaume, J.-L., Lambiotte, R., and Lefebvre, E. (2008). Fast Unfolding of Communities in Large Networks. *Journal of Statistical Mechanics: Theory and Experiment*. P10008. https://doi.org/10.1088/1742-5468/2008/10/p10008.

Bollmann, S., Puckett, A.M., Cunnington, R., Barth, M. (2018). Serial correlations in single-subject fMRI with sub-second TR. *Neuroimage, 166*(1), 152-166. https://doi.org/10.1016/j.neuroimage.2017.10.043.

Brun, V. H., Solstad, T., Kjelstrup, K. B., Fyhn, M., Witter, M. P., Moser, E. I., & Moser, M. B. (2008). Progressive increase in grid scale from dorsal to ventral medial entorhinal cortex. *Hippocampus*, *18*(12), 1200-1212.

Brunec, I. K., Bellana, B., Ozubko, J. D., Man, V., Robin, J., Liu, Z. X., Grady, C., … & Moscovitch, M. (2018). Multiple scales of representation along the hippocampal anteroposterior axis in humans. *Current Biology, 28*(13): 2129–2135. https://doi.org/10.1016/j.cub.20_18.05.016

Brunec, I. K., & Momennejad, I. (2019). Predictive representations in hippocampal and prefrontal hierarchies. *bioRxiv*, 786434.

Bullmore, E., Long, C., Suckling, J., Fadili, J., Calvert, G., Zelaya, F., ... & Brammer, M. (2001). Colored noise and computational inference in neurophysiological (fMRI) time series analysis: resampling methods in time and wavelet domains. *Human brain mapping*, *12*(2), 61-78.

Campbell, K., Grigg, O., Saverino, C., Churchill, N., & Grady, C. (2013). Age differences in the intrinsic functional connectivity of default network subsystems. *Frontiers in aging neuroscience*, *5*, 73. https://doi.org/10.3389/fnagi.2013.00073

Cavanagh, S. E., Wallis, J. D., Kennerley, S. W., & Hunt, L. T. (2016). Autocorrelation structure at rest predicts value correlates of single neurons during reward-guided choice. *elife*, *5*, e18937. https://doi.org/10.7554/eLife.18937.

Collin, S. H., Milivojevic, B., & Doeller, C. F. (2015). Memory hierarchies map onto the hippocampal long axis in humans. *Nature neuroscience*, *18*(11), 1562-1564. https://doi.org/10.1038/nn.4138

Cox, R. W. (1996). AFNI: software for analysis and visualization of functional magnetic resonance neuroimages. *Computers and Biomedical research*, *29*(3), 162-173.

Doeller, C. F., King, J. A., & Burgess, N. (2008). Parallel striatal and hippocampal systems for landmarks and boundaries in spatial memory. *Proceedings of the National Academy of Sciences*, *105*(15), 5915-5920. https://doi.org/10.1073/pnas.0801489105

DuBrow S, Davachi L. (2013). The influence of context boundaries on memory for the sequential order of events. *J Exp Psychol Gen, 142*(4), 1277-86. doi: 10.1037/a0034024.

Evensmoen, H. R., Lehn, H., Xu, J., Witter, M. P., Nadel, L., & Håberg, A. K. (2013). The anterior hippocampus supports a coarse, global environmental representation and the posterior hippocampus supports fine-grained, local environmental representations. *Journal of cognitive neuroscience*, *25*(11), 1908-1925. https://doi.org/10.1162/jocn_a_00436

Ezzyat Y, Davachi L. (2014). Similarity breeds proximity: pattern similarity within and across contexts is related to later mnemonic judgments of temporal proximity. *Neuron, 81*(5), 1179-1189. doi: 10.1016/j.neuron.2014.01.042.

Glasser, M. F., Smith, S. M., Marcus, D. S., Andersson, J. L., Auerbach, E. J., Behrens, T. E., ... & Van Essen, D. C. (2016). The human connectome project's neuroimaging approach. *Nature neuroscience*, *19*(9), 1175-1187. https://doi.org/10.1038/nn.4361

Glasser, M. F., Sotiropoulos, S. N., Wilson, J. A., Coalson, T. S., Fischl, B., Andersson, J. L., ... & Wu-Minn HCP Consortium. (2013). The minimal preprocessing pipelines for the Human Connectome Project. *Neuroimage*, *80*, 105-124. https://doi.org/10.1016/j.neuroimage.2013.04.127

Grady, C. L. (2020). Meta-analytic and functional connectivity evidence from functional magnetic resonance imaging for an anterior to posterior gradient of function along the hippocampal axis. *Hippocampus*, *30*(5), 456-471. https://doi.org/10.1002/hipo.23164

Gothard, K. M., Skaggs, W. E., & McNaughton, B. L. (1996). Dynamics of mismatch correction in the hippocampal ensemble code for space: interaction between path integration and environmental cues. *Journal of Neuroscience*, *16*(24), 8027-8040. https://doi.org/10.1523/JNEUROSCI.16-24-08027.1996

Griffanti, L., Salimi-Khorshidi, G., Beckmann, C. F., Auerbach, E. J., Douaud, G., Sexton, C. E., ... & Smith, S. M. (2014). ICA-based artefact removal and accelerated fMRI acquisition for improved resting state network imaging. *Neuroimage*, *95*, 232-247. https://doi.org/10.1016/j.neuroimage.2014.03.034

Hafting, T., Fyhn, M., Molden, S., Moser, M. B., & Moser, E. I. (2005). Microstructure of a spatial map in the entorhinal cortex. *Nature*, *436*(7052), 801-806. https://doi.org/10.1038/nature03721

Hasselmo, M. E. (2008). Grid cell mechanisms and function: contributions of entorhinal persistent spiking and phase resetting. *Hippocampus*, *18*(12), 1213-1229. https://doi.org/10.1002/hipo.20512

Hirshhorn, M., Grady, C., Rosenbaum, R. S., Winocur, G., & Moscovitch, M. (2012). Brain regions involved in the retrieval of spatial and episodic details associated with a familiar environment: an fMRI study. *Neuropsychologia*, *50*(13), 3094-3106. https://doi.org/10.1016/j.neuropsychologia.2012.08.008

Hrybouski, S., MacGillivray, M., Huang, Y., Madan, C. R., Carter, R., Seres, P., & Malykhin, N. V. (2019). Involvement of hippocampal subfields and anterior-posterior subregions in encoding and retrieval of item, spatial, and associative memories: longitudinal versus transverse axis. *NeuroImage*, *191* (1), 568-586. https://doi.org/10.1016/j.neuroimage.2019.01.061

Igarashi, K. M., Ito, H. T., Moser, E. I., & Moser, M. B. (2014). Functional diversity along the transverse axis of hippocampal area CA1. *FEBS letters*, *588*(15), 2470-2476. https://doi.org/10.1016/j.febslet.2014.06.004

Irish, M., & Vatansever, D. (2020). Rethinking the episodic-semantic distinction from a gradient perspective. *Current Opinion in Behavioral Sciences*, *32*, 43-49. https://doi.org/10.1016/j.cobeha.2020.01.016

Jacob, A. D., & Josselyn, S. A. (2020). Why Have Two When One Will Do? Comparing Task Representations across Amygdala and Prefrontal Cortex in Single Neurons and Neuronal Populations. *Neuron*, *107*(4), 597-599. https://doi.org/10.1016/j.neuron.2020.07.038

James, O., Park, H., & Kim, S. G. (2019). Impact of sampling rate on statistical significance for single subject fMRI connectivity analysis. *Human brain mapping*, *40*(11), 3321-3337. https://doi.org/10.1002/hbm.24600.

Jung, M. W., Wiener, S. I., & McNaughton, B. L. (1994). Comparison of spatial firing characteristics of units in dorsal and ventral hippocampus of the rat. *Journal of Neuroscience*, *14*(12), 7347-7356.

1181 Kjelstrup, K. B., Solstad, T., Brun, V. H., Hafting, T., Leutgeb, S., Witter, M. P., ... &
1182 Moser, M. B. (2008). Finite scale of spatial representation in the
1183 hippocampus. *Science*, *321*(5885), 140-143.
1184 https://doi.org/10.1126/science.1157086
1185
1186 Kok, P., Rait, L. I., & Turk-Browne, N. B. (2020). Content-based dissociation of
1187 hippocampal involvement in prediction. *Journal of Cognitive Neuroscience*, *32*(3),
1188 527-545. https://doi.org/10.1162/jocn_a_01509
1189
1190 Komorowski, R. W., Garcia, C. G., Wilson, A., Hattori, S., Howard, M. W., &
1191 Eichenbaum, H. (2013). Ventral hippocampal neurons are shaped by experience
1192 to represent behaviorally relevant contexts. *Journal of Neuroscience*, *33*(18),
1193 8079-8087. https://doi.org/10.1523/JNEUROSCI.5458-12.2013
1194
1195 Kyle, C. T., Stokes, J. D., Lieberman, J. S., Hassan, A. S., & Ekstrom, A. D. (2015).
1196 Successful retrieval of competing spatial environments in humans involves
1197 hippocampal pattern separation mechanisms. *Elife*, *4*, e10499.
1198 https://doi.org/10.7554/eLife.10499
1199
1200 Laurens R Krol (2021). Permutation Test (https://github.com/lrkrol/permutationTest),
1201 GitHub. Retrieved February 16, 2021.
1202
1203 Lee, A. C., Yeung, L. K., & Barense, M. D. (2012). The hippocampus and visual
1204 perception. *Frontiers in human neuroscience*, *6*, 91.
1205 https://doi.org/10.3389/fnhum.2012.00091
1206
1207 Lenoski, B., Baxter, L. C., Karam, L. J., Maisog, J., & Debbins, J. (2008). On the
1208 performance of autocorrelation estimation algorithms for fMRI analysis. *IEEE*
1209 *Journal of Selected Topics in Signal Processing*, *2*(6), 828-838.
1210 https://doi.org/10.1109/jstsp.2008.2007819.
1211
1212 Leutgeb, S., Leutgeb, J. K., Treves, A., Moser, M. B., & Moser, E. I. (2004). Distinct
1213 ensemble codes in hippocampal areas CA3 and CA1. *Science*, *305*(5688), 1295-
1214 1298. https://doi.org/10.1126/science.1100265
1215
1216 Lund, T. E., Madsen, K. H., Sidaros, K., Luo, W. L., & Nichols, T. E. (2006). Non-white
1217 noise in fMRI: does modelling have an impact? *Neuroimage*, *29*(1), 54-66.
1218 https://doi.org/10.1016/j.neuroimage.2005.07.005.
1219
1220 Maass, A., Berron, D., Libby, L. A., Ranganath, C., & Düzel, E. (2015). Functional
1221 subregions of the human entorhinal cortex. *Elife*, *4*, e06426.
1222 https://doi.org/10.7554/eLife.06426
1223
1224 Maurer, A. P., VanRhoads, S. R., Sutherland, G. R., Lipa, P., & McNaughton, B. L.
1225 (2005). Self-motion and the origin of differential spatial scaling along the septo-
1226 temporal axis of the hippocampus. *Hippocampus*, *15*(7), 841-852.
1227 https://doi.org/10.1002/hipo.20114
1228
1229 Montchal, M. E., Reagh, Z. M., & Yassa, M. A. (2019). Precise temporal memories are
1230 supported by the lateral entorhinal cortex in humans. *Nature neuroscience*, *22*(2),
1231 284-288. https://doi.org/10.1038/s41593-018-0303-1

Morrissey, M. D., Insel, N., & Takehara-Nishiuchi, K. (2017). Generalizable knowledge outweighs incidental details in prefrontal ensemble code over time. *Elife*, *6*, e22177. https://doi.org/10.7554/eLife.22177

Nadel, L., Hoscheidt, S., & Ryan, L.R. (2013). Spatial cognition and the hippocampus: the anterior–posterior axis. *Journal of Cognitive Neuroscience, 25*(1), 22-28. https://doi.org/10.1162/jocn_a_00313.

Navarro Schröder, T., Haak, K. V., Jimenez, N. I. Z., Beckmann, C. F., & Doeller, C. F. (2015). Functional topography of the human entorhinal cortex. *Elife*, *4*, e06738. https://doi.org/10.7554/eLife.06738

Nielson, D. M., Smith, T. A., Sreekumar, V., Dennis, S., & Sederberg, P. B. (2015). Human hippocampus represents space and time during retrieval of real-world memories. *Proceedings of the National Academy of Sciences*, *112*(35), 11078-11083. https://doi.org/10.1073/pnas.1507104112

Nilssen, E. S., Doan, T. P., Nigro, M. J., Ohara, S., & Witter, M. P. (2019). Neurons and networks in the entorhinal cortex: A reappraisal of the lateral and medial entorhinal subdivisions mediating parallel cortical pathways. *Hippocampus*, *29*(12), 1238-1254. https://doi.org/10.1002/hipo.23145

Olsen, R. K., Yeung, L. K., Noly-Gandon, A., D'Angelo, M. C., Kacollja, A., Smith, V. M., ... & Barense, M. D. (2017). Human anterolateral entorhinal cortex volumes are associated with cognitive decline in aging prior to clinical diagnosis. *Neurobiology of aging*, *57*, 195-205. https://doi.org/10.1016/j.neurobiolaging.2017.04.025

Peer, M., Ron, Y., Monsa, R., & Arzy, S. (2019). Processing of different spatial scales in the human brain. *Elife*, *8*, e47492. https://doi.org/10.7554/eLife.47492

Poppenk, J., Evensmoen, H. R., Moscovitch, M., & Nadel, L. (2013). Long-axis specialization of the human hippocampus. *Trends in cognitive sciences*, *17*(5), 230-240. https://doi.org/10.1016/j.tics.2013.03.005

Power, J. D., Barnes, K. A., Snyder, A. Z., Schlaggar, B. L., & Petersen, S. E. (2012). Spurious but systematic correlations in functional connectivity MRI networks arise from subject motion. *Neuroimage*, *59*(3), 2142-2154. https://doi.org/10.1016/j.neuroimage.2011.10.018

Purdon, P. L., & Weisskoff, R. M. (1998). Effect of temporal autocorrelation due to physiological noise and stimulus paradigm on voxel-level false-positive rates in fMRI. *Human brain mapping*, *6*(4), 239-249. https://doi.org/10.1002/(SICI)1097-0193(1998)6:4<239::AID-HBM4>3.0.CO;2-4

R Core Team (2019). R: A language and environment for statistical computing. R Foundation for Statistical Computing, Vienna, Austria. URL https://www.R-project.org/.

Rajapakse, J. C., Kruggel, F., Maisog, J. M., & Yves von Cramon, D. (1998). Modeling hemodynamic response for analysis of functional MRI time-series. *Human brain*

mapping, *6*(4), 283-300. https://doi.org/3.0.co;2-#">10.1002/(sici)1097-0193(1998)6:4<283::aid-hbm7>3.0.co;2-#

Raut, R. V., Snyder, A. Z., & Raichle, M. E. (2020). Hierarchical dynamics as a macroscopic organizing principle of the human brain. *Proceedings of the National Academy of Sciences*, *117*(34), 20890-20897. https://doi.org/10.1073/pnas.2003383117

Robin, J., & Moscovitch, M. (2017). Details, gist and schema: hippocampal–neocortical interactions underlying recent and remote episodic and spatial memory. *Current opinion in behavioral sciences*, *17*, 114-123. https://doi.org/10.1016/j.cobeha.2017.07.016

Salimi-Khorshidi, G., Douaud, G., Beckmann, C. F., Glasser, M. F., Griffanti, L., & Smith, S. M. (2014). Automatic denoising of functional MRI data: combining independent component analysis and hierarchical fusion of classifiers. *Neuroimage*, *90*, 449-468. https://doi.org/10.1016/j.neuroimage.2013.11.046

Schapiro, A. C., Turk-Browne, N. B., Botvinick, M. M., & Norman, K. A. (2017). Complementary learning systems within the hippocampus: a neural network modelling approach to reconciling episodic memory with statistical learning. *Philosophical Transactions of the Royal Society B: Biological Sciences*, *372*(1711), 20160049.

Singmann, H., Bolker, B., Westfall, J., Aust, F., & Ben-Shachar, M. S. (2020). afex: Analysis of Factorial Experiments. R package version 0.28-0. https://CRAN.R-project.org/package=afex

Smith, S. M., Beckmann, C. F., Andersson, J., Auerbach, E. J., Bijsterbosch, J., Douaud, G., ... & WU-Minn HCP Consortium. (2013). Resting-state fMRI in the human connectome project. *Neuroimage*, *80*, 144-168.https://doi.org/10.1016/j.neuroimage.2013.05.039.

Strange, B. A., Witter, M. P., Lein, E. S., & Moser, E. I. (2014). Functional organization of the hippocampal longitudinal axis. *Nature Reviews Neuroscience*, *15*(10), 655-669. https://doi.org/10.1038/nrn3785

Tsao, A., Sugar, J., Lu, L., Wang, C., Knierim, J. J., Moser, M. B., & Moser, E. I. (2018). Integrating time from experience in the lateral entorhinal cortex. *Nature*, *561*(7721), 57-62. https://doi.org/10.1038/s41586-018-0459-6

Vaidya, A. R., & Badre, D. (2020). Neural systems for memory-based value judgment and decision-making. *Journal of cognitive neuroscience*, *32*(10), 1896–1923. https://doi.org/10.1162/jocn_a_01595

Van Essen, D. C., Smith, S. M., Barch, D. M., Behrens, T. E., Yacoub, E., Ugurbil, K., & Wu-Minn HCP Consortium. (2013). The WU-Minn human connectome project: an overview. *Neuroimage*, *80*, 62-79. https://doi.org/10.1016/j.neuroimage.2013.05.041.

Wickham, H. (2017). tidyverse: Easily Install and Load the 'Tidyverse'. R package version 1.2.1. https://CRAN.R-project.org/package=tidyverse

1334 Wickramaarachchi, C., Frincu, M., Small, P., & Prasanna, V. K. (2014, September). Fast
1335 parallel algorithm for unfolding of communities in large graphs. In *2014 IEEE*
1336 *High Performance Extreme Computing Conference (HPEC)* (pp. 1-6). IEEE.
1337 https://doi.org/10.1109/hpec.2014.7040973.
1338
1339 Witter, M. P., & Amaral, D. G. (2021). The entorhinal cortex of the monkey: VI.
1340 Organization of projections from the hippocampus, subiculum, presubiculum, and
1341 parasubiculum. *Journal of Comparative Neurology*, *529*(4), 828-852.
1342 https://doi.org/10.1002/cne.24983
1343
1344 Witter, M. P., Doan, T. P., Jacobsen, B., Nilssen, E. S., & Ohara, S. (2017). Architecture
1345 of the entorhinal cortex a review of entorhinal anatomy in rodents with some
1346 comparative notes. *Frontiers in Systems Neuroscience*, *11*, 46.
1347 https://doi.org/10.3389/fnsys.2017.00046.
1348
1349 Yassa, M. A., & Stark, C. E. (2011). Pattern separation in the hippocampus. *Trends in*
1350 *neurosciences*, *34*(10), 515-525. https://doi.org/10.1016/j.tins.2011.06.006
1351
1352 Yeung, L. K., Olsen, R. K., Hong, B., Mihajlovic, V., D'Angelo, M. C., Kacollja, A., ... &
1353 Barense, M. D. (2019). Object-in-place memory predicted by anterolateral
1354 entorhinal cortex and parahippocampal cortex volume in older adults. *Journal of*
1355 *Cognitive Neuroscience*, *31*(5), 711-729. https://doi.org/10.1162/jocn_a_01385
1356
1357 Yeung, L. K., Olsen, R. K., Bild-Enkin, H. E., D'Angelo, M. C., Kacollja, A., McQuiggan,
1358 D. A., ... & Barense, M. D. (2017). Anterolateral entorhinal cortex volume
1359 predicted by altered intra-item configural processing. *Journal of*
1360 *Neuroscience*, *37*(22), 5527-5538. https://doi.org/10.1523/JNEUROSCI.3664-
1361 16.2017